10.1098/rsta.2004.1444

THE ROYAL SOCIETY

Resonant Raman spectroscopy of nanotubes

By Christian Thomsen[1], Stephanie Reich[2] and Janina Maultzsch[1]

[1]*Technische Universität Berlin, Hardenbergstraße 36, 10623 Berlin, Germany*
[2]*Department of Engineering, University of Cambridge, Trumpington Street, Cambridge CB2 1PZ, UK* (sr379@eng.cam.ac.uk)

Published online 28 September 2004

Single and double resonances in Raman scattering are introduced and six criteria for the observation and identification of double resonances stated. The experimental situation in carbon nanotubes is reviewed in view of these criteria. The evidence for the D mode and the high-energy mode is found to be overwhelming for a double-resonance process to take place, whereas the nature of the radial breathing-mode Raman process remains undecided at this point. Consequences for the application of Raman scattering to the characterization of nanotubes are discussed.

Keywords: carbon nanotubes; double resonance; Raman scattering; defects

1. Introduction

Raman scattering in carbon nanotubes has developed into a method of choice in the investigation of their physical properties and their characterization. The study of electronic resonances in the Raman spectra, a method which has been used extensively, for example, in work on semiconductors (Cardona 1982), gives us a wealth of information about the electronic band structure of a material. This is also true for the Raman work on carbon nanotubes, where resonance studies have moved into the focus of research.

Traditional Raman studies of carbon nanotubes focus on the radial breathing mode (RBM), a mode where all atoms vibrate in phase in the radial direction (Dresselhaus *et al.* 1995). Its frequency, as can easily be shown (Jishi *et al.* 1993), depends inversely on the diameter of the tube and is thus a straightforward tool for finding the diameter of an isolated nanotube. One consequence arising specifically from Raman resonances is that the RBM only appears strong enough in the spectra when the incident (or scattered) laser energy coincides with an electronic transition in the nanotube. Jorio *et al.* (2001) have used this property to map the joint electronic density of states in a collection of isolated nanotubes by analysing the Raman intensity of the RBM in Stokes and anti-Stokes scattering as a function of laser energy. The underlying assumption when doing so is that a single resonance prevails in the RBM Raman scattering process.

The two other energy regions of most interest in the first-order Raman spectra when studying electronic resonances are the D mode (around 1200 cm^{-1}) and the

One contribution of 13 to a Theme 'Raman spectroscopy in carbons: from nanotubes to diamond'.

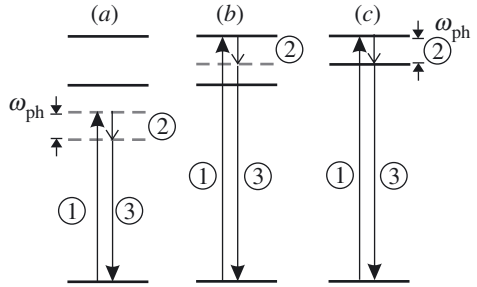

Figure 1. Schematic of (*a*) a non-resonant process, (*b*) a single-resonance (Stokes) process, and (*c*) higher-order resonance (Stokes) process in Raman scattering. Actually shown in (*c*) is a triple-resonance process; in double-resonance with elastic defect scattering another virtual state with an energy equal to one of the phonon eigenstates is involved before recombination. (Reproduced with permission from Reich *et al.* (2004).)

high-energy mode (HEM) (at 1590 cm^{-1}). An important point for the understanding of the Raman spectra is that they originate from double resonances (Maultzsch *et al.* 2001, 2002*a*, 2003). While this fact is generally accepted for the D mode, there is still some debate over the origin of the HEM (see, for example, Jorio *et al.* 2003). The experimental evidence, however, is overwhelming that the HEM—at least predominantly—is a double-resonance process as well.

We will present the concept of single and double resonances in Raman scattering in general and give a consistent interpretation of the experimental results found on nanotubes in terms of double resonances. An explicit discussion of where the single resonance picture fails, and where its strengths are, can be found in the book by Reich *et al.* (2004) and other articles in this issue, respectively.

2. Resonances in first-order Raman scattering

Resonant Raman scattering is characterized by a strong enhancement of the detected intensity when real transitions are involved in the Raman process. The conceptual difference between non-resonant, single-resonance and double-resonance Raman processes is best illustrated in the energy schematic of figure 1. Each solid (horizontal) line indicates an eigenstate of the system to be studied. A non-resonant process (*a*) does not involve the excited eigenstates; the incoming photon is absorbed and places the excited electron into a virtual state (grey dashed line, transition 1), a phonon is emitted (transition 2) and the electron is now in a second virtual (lower) state. From there it can recombine (transition 3) and the Raman shifted photon is emitted. In total six different time orders contribute to this process, of which we show only one.

A single resonance occurs if one of the intermediate states of the excited electron is an eigenstate of the system (see figure 1*b*). Here the incoming light is chosen such that the electron is excited into the upper eigenstate of the system (transition 1), the phonon emission puts it into a virtual state (transition 2), and recombination into the ground state occurs from there (transition 3). The Raman enhancement when matching a real state is seen from the expression for single-resonance scattering $K_{2\mathrm{f},10}$ of the process in figure 1*b* (Martin & Falicov 1983):

$$K_{2\mathrm{f},10} = \sum_{a,b} \frac{\langle \omega_{2,f,i}|H_{\mathrm{eR},\rho}|0,f,b\rangle\langle 0,f,b|H_{\mathrm{ep}}|0,0,a\rangle\langle 0,0,a|H_{\mathrm{eR},\sigma}|\omega_1,0,i\rangle}{(E_1 - E^{\mathrm{e}}_{ai} - \mathrm{i}\gamma)(E_1 - \hbar\omega - E^{\mathrm{e}}_{bi} - \mathrm{i}\gamma)}, \qquad (2.1)$$

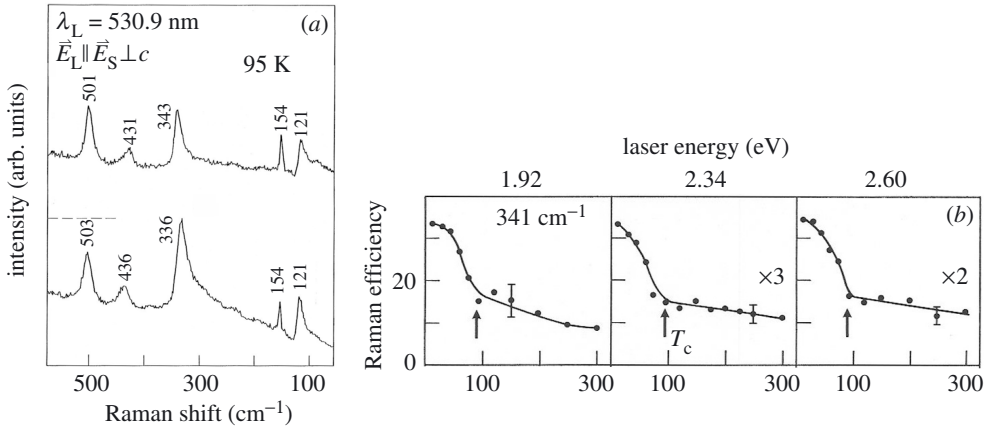

Figure 2. A resonance of the Raman active phonon with the superconducting energy gap in $YBa_2Cu_3O_7$. (*a*) Spectra of the five A_{1g} phonons slightly above the superconducting transition temperature (upper curve) and at temperatures much below T_c (lower curve). Note the strong increase in intensity of the mode at 340 cm^{-1}. (*b*) Temperature dependence of the Raman efficiency, which is the Raman intensity normalized by $[\omega_s^4(n(\omega_{ph}, T) + 1)]$. The enhancement of the Raman efficiency is independent of the excitation energy and occurs below T_c, as indicated by the arrows. $\vec{E}_L$ and $\vec{E}_S$ refer to the polarization of the incident laser and the scattered light, respectively. They are both perpendicular to the *c*-axis of the cup. (After Friedl *et al.* (1991).)

where $|\omega_1, 0, i\rangle$ denotes the state with an incoming photon of energy $E_1 = \hbar\omega_1$, the ground state 0 of the phonon (no phonon excited), and the ground electronic state i; the other states are labelled accordingly. The initial and final electronic states are assumed to be the same; the sum is over all possible intermediate electronic states a and b. The final phononic state is denoted by f. The E^e_{ai} are the energy differences between the electronic states a and i; the lifetime of the various excited states γ is taken to be the same.

Figure 1*b* corresponds to the incoming photon with energy E_1 matching the energy of the electronic state E^e_{ai} in equation (2.1). The matrix element would be seen to diverge if it were not for the (imaginary) lifetime part. As the incoming light is in resonance, the situation in figure 1*b* is referred to as incoming (single) resonance. One speaks of an outgoing resonance when the photon emitted in the recombination process matches an eigenenergy of the system, i.e. $E_1 - \hbar\omega_{ph} = E^e_{bi}$. The Raman intensity is given by the square of $K_{2f,10}$, leading to the strong enhancements in the spectra when the incoming (or outgoing) photon energies are matched to the eigenenergies of the investigated system. It is obvious that by using appropriate energies of tunable lasers the real electronic states of a material can be studied systematically. The authoritative work on solid-state systems using this technique has been performed by Cardona (1982).

An example where the emitted *phonon* (rather than incoming or outgoing photon) matches a transition between eigenstates in a system was shown by Friedl *et al.* (1991) in a temperature-dependent study of the high-temperature superconductor $YBa_2Cu_3O_7$ (see figure 2). Contrary to what is normally expected in temperature-dependent Raman spectra, in this system, the intensity of the Raman active phonon at $\omega_{ph} \approx 340$ cm^{-1} is greatly enhanced below the superconducting transition temperature T_c. This enhancement is roughly independent of excitation energy: see figure 2*b*,

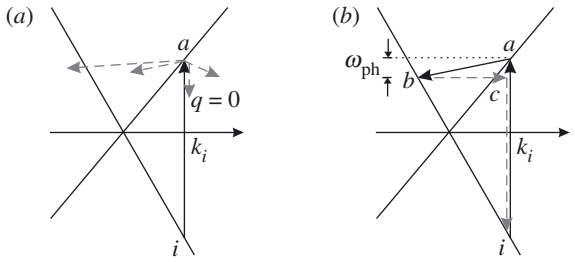

Figure 3. Different resonant processes in systems with linear electronic bands: a good approximation for graphite or metallic nanotubes. (*a*) Single resonance; only the incoming light is resonant ($i \to a$), the possibly emitted phonons and the recombination are not. (*b*) Double resonance; the incident photon ($i \to a$) and the emitted phonon ($a \to b$) make transitions between eigenstates of the system; the elastic (defect) scattering ($b \to c$) and the recombination ($c \to i$) do not. (After Reich *et al.* (2004).)

which excludes an incoming or outgoing (photon) resonance. Instead, one of the terms with different time order has a denominator proportional to $[2\Delta(T) - \hbar\omega_{\mathrm{ph}}]$, which comes to resonance when the superconducting gap 2Δ develops as a function of temperature below T_{c}. The phonon at $\omega_{\mathrm{ph}} \approx 340\,\mathrm{cm}^{-1}$ matches best the gap energy and thus the Raman efficiency of this phonon is enhanced at low temperatures (for details, see Friedl *et al.* 1990, 1991).

Apart from the energy conservation ($\hbar\omega_1 = \hbar\omega_2 \pm \hbar\omega_{\mathrm{ph}}$) we must consider momentum conservation in the Raman processes. For the first-order Raman term (equation (2.1)) this implies that

$$\boldsymbol{q}_1 = \boldsymbol{q}_2 \pm \boldsymbol{q}_{\mathrm{ph}} \tag{2.2}$$

must be fulfilled, leading to the usual Raman rule that only phonons with very small momentum ($q_{\mathrm{ph}} \approx 0$, Γ-point phonons) are observed when exciting with visible light because of its small momentum. This restriction can be circumvented by using photons with large momenta, comparable with that of the Brillouin zone of the solid. Recently, Maultzsch *et al.* (2004) used X-rays as the light source for first-order Raman scattering, allowing the momenta of the incoming and scattered photon to be chosen in such a way that the entire in-plane optical-phonon dispersion of graphite could be measured, following the initial X-ray work on diamond and GaN (Ruf *et al.* 2001; Schwoerer-Böhning *et al.* 1998).

Graphite and metallic carbon nanotubes have the specific and common property that their electronic bands in the visible region are strongly dispersive; their dispersion near the Fermi surface is in fact nearly linear, and the schematic in figure 3 describes the possible transitions in the Raman process in graphite and metallic nanotubes. In figure 3*a* we show the resonant incoming photon absorption as a vertical arrow. Note that that transition is resonant regardless of the photon energy. Every photon can make such a resonance because of the monotonically increasing energy of the electronic bands. The emitted phonons (grey dashed arrows) correspond to various possible non-resonant carrier scattering processes. The recombination between eigenstates occurs again such that equation (2.2) is fulfilled, i.e. only a $q \approx 0$ phonon can occur in a single-resonance process. In general, as long as the phonon emission is not tied to another transition of an electron or hole to an eigenstate of the system, one speaks of a single-resonance Raman process. Compared with non-resonance Raman

spectra (figure 1*a*), the only essential difference in single-resonance spectra (figures 1*b* and 3*a*) is the large intensity enhancement according to the vanishing denominator in equation (2.1). Often this enhancement is needed to make the excitation at all detectable in the Raman spectra.

3. Resonances in higher-order Raman scattering

In analogy to single-resonance scattering one speaks of a double resonance, when *two* of the transitions involve excited eigenstates of the investigated system, and a triple resonance when *three* transitions are real (figure 1*c*). These multiple resonances have also been observed in solids before, but it is clear that the photon and phonon energies involved must both match quite well the electronic system for a multiple resonance to occur. Experimentally, a double resonance was achieved for some specific settings of parameters, for example, by tuning the eigenenergies in a magnetic field or by applying pressure (see Gubarev *et al.* 1991; Sapega *et al.* 1992).

With the many possible non-resonantly emitted phonons in figure 3*a*, there exists also the possibility of scattering the electron from eigenstate a to another eigenstate, b say, on the other (linear) band (figure 3*b*), adding a second resonance to the Raman process. Note that this process is only allowed for a particular combination of energy and momentum of the phonon that scatters the electron. The specific energy–momentum relation of the phonon is, however, its dispersion relation, and it is in this way that phonons with a general quasi-momentum q, far from the Γ point, come into play in double-resonance processes. Of course, momentum has to be conserved in double resonance as well; the recombination must occur (for visible-light excitation) near the point in k-space where the initial absorption occurred. One way of scattering the electron back to k_i is to scatter it elastically off a defect, the other possibility is to scatter it with another phonon. The former process is indicated in figure 3*b* (process $b \to c$ runs horizontally, i.e. elastically); it is non-resonant, as c is not an eigenstate of the system, and recombination occurs from there, conserving (quasi-) momentum. The latter process involves the emission of another phonon, leading to a Raman signal at twice the phonon energy (second-order Raman scattering).

These processes are of second order and the Raman matrix element given by one more matrix element and one more resonant denominator than in first-order scattering (Martin & Falicov 1983; Thomsen & Reich 2000):

$$K_{2\mathrm{f},10} = \sum_{a,b,c} \frac{\mathcal{M}_{\mathrm{eR},\rho}\mathcal{M}_{\mathrm{e-def}}\mathcal{M}_{\mathrm{ep}}\mathcal{M}_{\mathrm{eR},\sigma}}{(E_1 - E^{\mathrm{e}}_{ai} - \mathrm{i}\gamma)(E_1 - \hbar\omega_{\mathrm{ph}} - E^{\mathrm{e}}_{bi} - \mathrm{i}\gamma)(E_1 - \hbar\omega_{\mathrm{ph}} - E^{\mathrm{e}}_{ci} - \mathrm{i}\gamma)}, \quad (3.1)$$

where we have abbreviated the matrix elements in the numerator by $\mathcal{M}_i$. Specifically, $\mathcal{M}_{\mathrm{e-def}}$ refers to the elastic interaction of the defect and the scattered electron. Not much is known about this interaction and the assumption that it is elastic and symmetry conserving for the scattered carrier is the simplest but not necessarily the only one. By Occam's razor we believe it to be the correct one. In analogy to the single-resonance term, the Raman intensity is strongly enhanced when the denominator goes to zero, i.e. when transitions between eigenstates take place in the process. As usual, all of these processes can occur in a different time order and for the hole instead of the electron. A full description takes all time orders and both carrier types into account.

The fascinating point about the double-resonance process is that a different incoming photon energy (say, $i' \rightarrow a'$) leads to a different excited electron. To fulfil the second resonant transition a phonon of different momentum and energy is now required. Specifically, a larger incoming photon energy requires a larger phonon momentum and—depending on the phonon dispersion—involves a higher or lower phonon energy. Scanning the incident photon energy thus corresponds to scanning the phonon energy in k-space. We will show this explicitly later, in figure 9, where an experimental energy scan is compared with a calculated wave vector scan of an isolated nanotube. The (approximate) phonon wave vectors are given and (in general not linearly) related to the incoming photon energy. Neglecting the phonon energy when compared with the much larger laser energy, the double-resonance phonon wave vector may be approximated by $q = 2k_i$. This relationship is often used for quick evaluation of the double-resonance conditions for different laser energies. For linear bands equation (3.1) can be evaluated analytically and a linear relation between incoming photon energy and phonon momentum may be found (see Thomsen & Reich 2000). Based on our double-resonance Raman interpretation, Saito *et al.* (2002) re-evaluated a selection of literature data and plotted them onto the phonon-dispersion curves of graphite. For a full analysis see Reich & Thomsen (2004). The phonon dispersion of an isolated nanotube was measured and evaluated using this technique by Maultzsch *et al.* (2003) (see figure 9).

We show here an example where double resonance was suggested by Mowbray *et al.* (1990) to be an explanation of an additional —i.e. not Raman allowed—mode in the Raman spectra of Ge reported by Gaisler *et al.* (1987). The additional mode, in energy below the Γ-point phonon of Ge, is seen in figure 4*a* as a small shoulder. Characteristic for all double-resonance processes is the excitation-energy dependence of the energy of the elementary excitation studied. It is clearly seen in figure 4*a* that the small peak shifts in energy with respect to the Γ-point phonon at $320\,\mathrm{cm}^{-1}$. Surprisingly, this shift depends on the surface of the Ge sample studied (figure 4*b*). The frequency separation from the Γ-point phonon increases approximately linearly, with the extrapolation to zero-shift intersecting the excitation-energy axis at E_1, the lowest direct gap of Ge (figure 4*b*). The three surfaces show different slopes in this plot.

The idea of the double-resonance process in Ge is that as soon as the excitation energy is large enough to make a direct transition there is the additional possibility of scattering an electron resonantly with a phonon across the band minimum, i.e. into an eigenstate (see figure 4*c*). Before recombination, the electron is scattered back into a virtual state, from where it can recombine with the excited hole. The slope of the excitation-energy dependence is given by the effective masses of the carriers in Ge, which is highly anisotropic near the critical point (for details, see Mowbray *et al.* 1990). The double-resonance process is a convolution of the phonon dispersion with the electronic dispersion, because the excited carrier is scattered to a second eigenstate of the system. In case of a known phonon dispersion, this process can thus be used to extract information about the electronic dispersion. In the case of Ge, Mowbray *et al.* (1990) derived the effective masses for the three principal directions in Ge. We see from this example that it is by no means necessary to have linear bands for a double resonance to occur; any strong dispersion suffices.

Another characteristic of a double resonance is the step before recombination. Generally it is sufficient for the twice-resonantly scattered carrier to make a transition

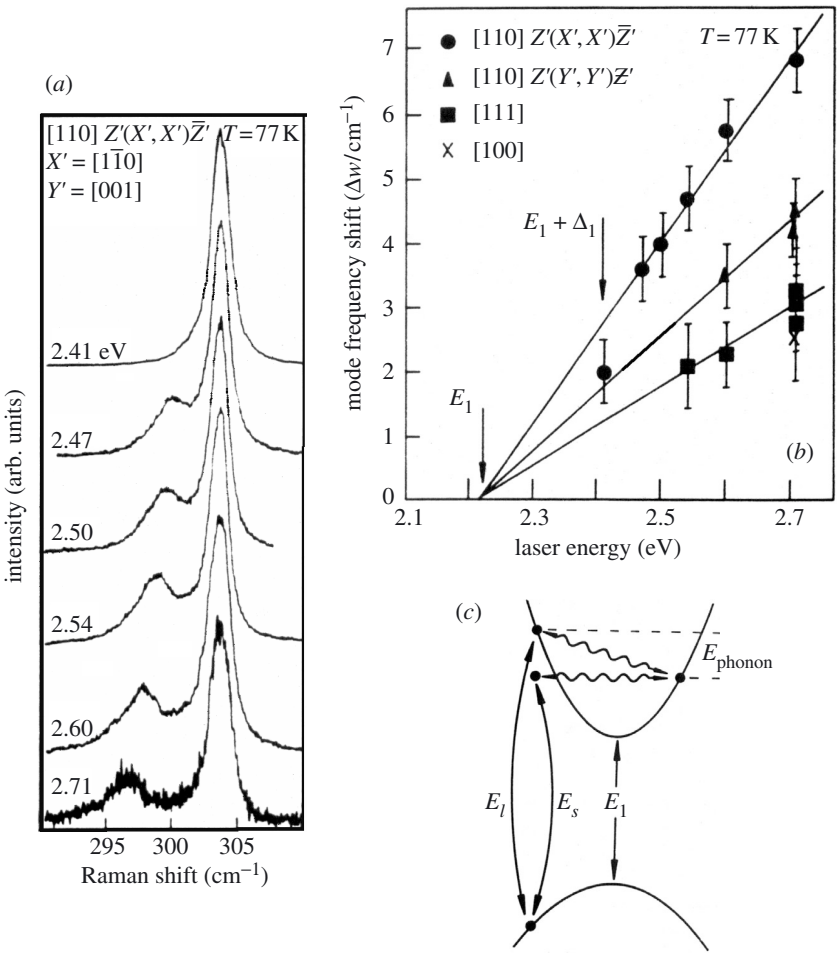

Figure 4. Double-resonance Raman scattering in Ge. The small shoulder in (*a*) and (*b*) has the characteristics of a double resonance: firstly, an excitation energy dependent shift; secondly, a shift which depends on the electronic structure (here surface) of the investigated material, and a symmetry-breaking element is involved to conserve quasi-momentum (here again the surface). In (*c*) we show a schematic of the double resonance. (After Mowbray *et al.* (1990).)

into a virtual state in order to conserve quasi-momentum in the entire process. In the case of Ge the scattering happens through the symmetry-breaking surface; the absorption depth of Ge at 2.5 eV is only *ca.* 160 Å, and the carriers 'feel' the surface. In graphite or carbon nanotubes this process is mediated by a defect or a second phonon (in second-order scattering). We focus now on double resonances in carbon nanotubes; for a review of double resonances in graphite, see Reich & Thomsen (2004).

4. Double resonances in carbon nanotubes

While we restrict ourselves here to resonances in carbon nanotubes we keep in mind that historically the excitation-energy dependent shift, which is *the* characteristic

feature of a double-resonance process, was first found in graphite by Vidano *et al.* (1981) and—only much later—explained by double-resonance scattering (Thomsen & Reich 2000). Given that the electronic band structures of carbon nanotubes and graphite are related through wrapping up a graphene sheet, it seems natural to look for the corresponding double-resonance process in nanotubes as well. This analogy is even more obvious as the unusual Raman feature of a strong excitation-energy dependent shift of one of the modes in graphite occurs with similar magnitude in the first- and second-order spectra of single-walled and multi-wall carbon nanotubes as well (Kastner *et al.* 1994; Thomsen 2000).

We summarize here the characteristics of a double resonance in solids; from what we know they always appear in a double-resonance process, although each individual characteristic cannot always be determined sufficiently accurately to conclude reliably the nature of the process from it alone:

(1) Dispersive electronic and phonon bands and

(2) a symmetry-breaking scattering process to conserve quasi-momentum (or a higher-order scattering with two or more phonons), resulting in

(3) an excitation-energy dependence of the Raman peak position,

(4) not necessarily simple Lorentzian line shapes,

(5) a comparatively large Raman intensity, and

(6) frequency and possible line shape differences in Stokes and anti-Stokes spectra.

Characteristics (1) and (2) are conditions for the double resonance to occur, the others ((3)—(6)) are experimental features from which a double resonance can be identified in Raman spectra. Each one of these experimental features may also have a different origin, for example, the non-Lorentzian line shape may result from interactions of the excitation with a continuum (Brown *et al.* 2001; Fano 1961; Jiang *et al.* 2002), or may be the result of two or more unresolved individual Lorentz peaks. The Raman intensity is generally difficult to determine reliably in absolute terms, and in order to quantify it relative to a second peak in the spectrum one has to be sure of the double or single-resonance nature of the second peak. All these features have been studied extensively in carbon nanotubes, and we will discuss them in what follows. They have been confirmed for the high-energy mode and the D mode, while we feel that the extent to which the RBM is double resonant is still unresolved. We discuss the three energy regions in order of decreasing frequency in the Raman spectrum.

Apart from the double-resonance process itself, the density of states may enhance the observed Raman intensity significantly. Generally speaking, the singularities in the electronic density of states of carbon nanotubes contribute most to the sum in equation (3.1). In the simplest view, one may say that *only* nanotubes where the incoming or outgoing light matches the singularity in the electronic joint density of states (to within some line width γ) are seen in the Raman spectra. When considering only single resonances this is an acceptable approximation—an approach taken, for example, by Jorio *et al.* (2001) when characterizing the joint density of states of an isolated nanotube over a small energy range. In a double-resonance process, however,

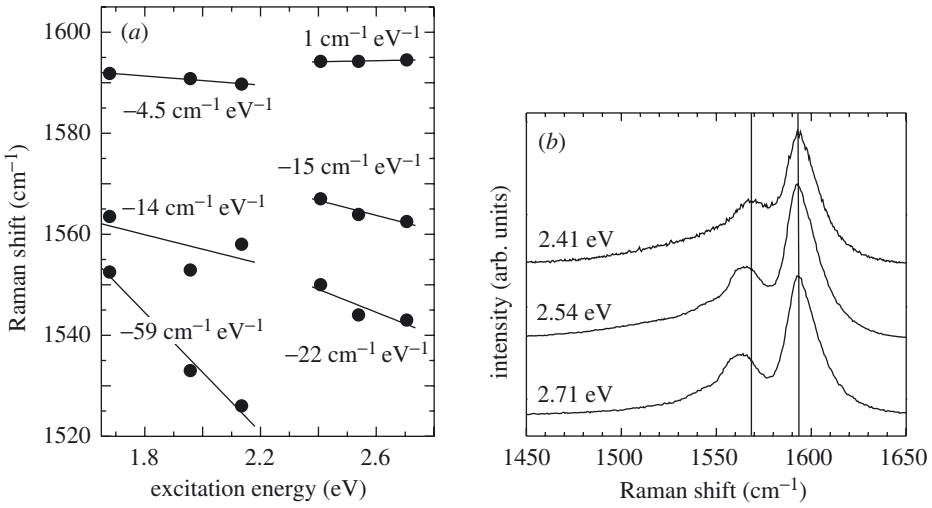

Figure 5. (*a*) Peak frequencies in the excitation energy range 1.7–2.7 eV. All peaks have an excitation-energy dependence, due to the double-resonance process. The jump in absolute phonon energies and slopes at 2.3 eV is due to a higher electronic band coming into double resonance, as explained by Maultzsch *et al.* (2002*a*). (*b*) Raman spectra of carbon nanotubes excited at three different laser energies. Clearly seen is the downshift of the second largest peak for increasing phonon energy. (Reproduced with permission from Thomsen (2003).)

the two simultaneously occurring resonances play a dominant role in determining the Raman intensity, which may not be ignored in the analysis. Note that in the sum of equation (3.1) the density-of-states effects are always explicitly included; they do not need separate consideration as is sometimes claimed (Kürti *et al.* 2002).

(*a*) *The energy shift and the defect-scattering mechanism*

Let us take a look at the features of a typical Raman spectrum of carbon nanotubes in figure 5. The dispersive nature of electron and phonon bands in nanotubes leads to shifts in the peak energies as shown in (*a*). The largest peak has the smallest energy dependence; those of the smaller satellites are larger. The shifts are negative and positive; both sign and magnitude depend on the details of the dispersions involved. Similar shifts in the high-energy mode were found by Jiang *et al.* (2003) although they have not been identified as due to double resonances. Criteria (1) and (3) are thus fulfilled. The symmetry-breaking process (2) responsible for scattering the excited carrier back (in k-space) to where it was excited ((*b*) → (*c*) in figure 1*b*) was identified in graphite by Tuinstra & Koenig (1970) (see also Wang *et al.* 1990). They found defects responsible for the amplitude of the D mode peak, and it is reasonable to assume the same for carbon nanotubes. Direct evidence for the intensity dependence of the high-energy mode (and the D mode) in multi-wall nanotubes was given in a defect-concentration dependent study by Maultzsch *et al.* (2002*c*). They showed that both high-energy and D mode intensity are proportional to the number of defects (given by the concentration of a dopant atom in the rods used for nanotube preparation). In an experiment where nanotubes were exposed to γ-irradiation, Skákalová *et al.* (2003) found qualitatively similar results. Other researchers have found a varying intensity of the high-energy mode when going along the tube with high spatial res-

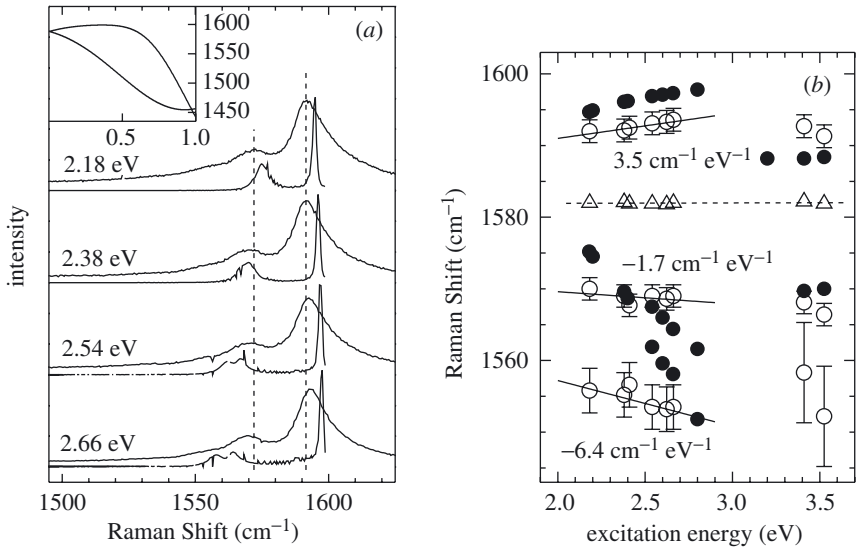

Figure 6. Comparison of the high-energy mode in theory and experiment. (*a*) The line shape and the splitting of the two components of the high-energy mode are nicely reproduced in the calculation. (*b*) The experimental frequencies—as with the case for the theoretical ones—are seen to exhibit positive and negative energy shifts as a function of excitation energy. While the highest mode agrees quantitatively, the two lower ones shift more strongly than observed. This may be due to the fact that we selected a specific tube $(15, 6)$ in the calculation while averaging over a sample distribution in the experiment. The frequencies of the graphite Γ-point phonon are shown for comparison (triangles). They do not exhibit any shift to within the accuracy of the experiment and must be assumed to originate from a single-resonance process. See text for details. (Reproduced with permission from Maultzsch *et al.* (2002*a*).)

olution (Jiang *et al.* 2003), consistent with a Raman intensity dependence on defect concentration. We thus consider criterion 2 to be fulfilled for a double-resonance process.

(*b*) *The Raman line shape*

Next, it is obvious that the line shape of the high-energy mode in figure 5*b* is not a simple Lorentzian (criterion 4). This fact has been known from the very beginning of nanotube research but has largely been ignored as an indicator for double-resonance scattering. The challenge of actually calculating the specific line shape from a given electronic band structure and a phonon dispersion was met by Maultzsch *et al.* (2002*a*), and the results are shown in figure 6*a*, where both the shift and the line shape of the high-energy Raman spectrum are calculated. These, and the work on metallic nanotubes by Jiang *et al.* (2002), are, to our knowledge, the only calculations of the line shape of the high-energy mode that are available. We find in agreement with the double resonance that: the highest peak frequency is *above* the Γ-point phonon frequency of graphite; the high-energy peak is split into two or more peaks with an intensity ratio quite close to that of the experiment; there are negative and positive slopes in the excitation-energy dependence of the peak frequencies. Quantitatively, the calculated values agree or are somewhat larger than what is

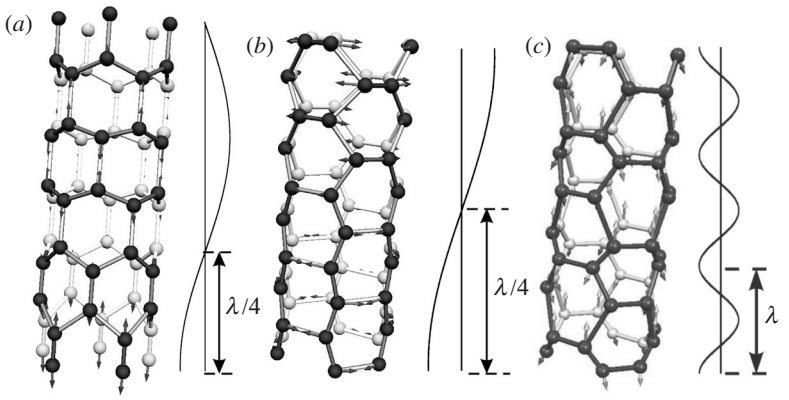

Figure 7. Phonon eigenvectors giving rise to the high-energy modes (a) and (b) and to the D mode (c). (a) Fully symmetric axial displacement (arrows) with wave vector $q \neq 0$ in a zig-zag tube. At the Γ point, this mode has A_{1g} symmetry. The wavelength of the vibration, which can be found from the nodes in the displacement magnitude, is indicated. (b) Fully symmetric circumferential vibration in an armchair tube (A_{1g} at the Γ point). (c) Vibration with $q = 4\pi/3a_0$ ($\lambda = 1.5a_0$), where a_0 is the lattice constant of graphite and of the armchair tube. It corresponds to the A_1' mode at the K point of graphite and gives rise (with q near $4\pi/3a_0$) to the D mode.

observed experimentally, see figure 6*b*, a fact which we have attributed to the presence of many tubes in the sample measured in figure 6*a*, whereas only a single tube of chirality $(15, 6)$ was taken into consideration in the calculation.

In isolated nanotubes the high-energy mode line width is indeed smaller, as was shown first by Duesberg *et al.* (2000) and corresponds much more to the calculation in figure 6.

The calculation in figure 6 includes only the two fully symmetric high-energy phonon branches of the $(15, 6)$ tube. Because of the double resonance, more than two peaks appear in the lower curves in figure 6. Thus the calculation is fully consistent with selection rules, which allow only $A_{1(g)}$ modes for light with parallel polarization to the tube axis. The eigenvectors giving rise to the high-energy modes are shown schematically in figure 7*a*, *b*. They are non-Γ point modes according to the double resonance (see the indicated wavelength). In zig-zag tubes, the axial vibration is Raman allowed (figure 7*a*), whereas in armchair tubes the circumferential vibration contributes to the high-energy peak (figure 7*b*). In chiral nanotubes, both vibrations are Raman active; the eigenvectors can mix and lose their purely longitudinal or transverse character (Reich *et al.* 2001*b*). Figure 7*c* shows the displacement with wavelength $\lambda = 1.5a_0$ corresponding to the A_1' phonon at the K point in graphite. The corresponding displacements with $\lambda \approx 1.5a_0$ result in the D mode (see also § 6).

(*c*) *The Raman intensity*

Criterion 5 for a double resonance considers the comparatively large Raman peak intensity. Qualitatively speaking, the Raman signal in nanotubes is quite intense; single isolated nanotubes, as mentioned, can be detected without much difficulty in a standard Raman set-up. However, it is difficult to give a serious estimate of the Raman intensity, since experimentally it is convoluted with the detector and spectrometer sensitivities as well as the aperture and quality of the Raman collection

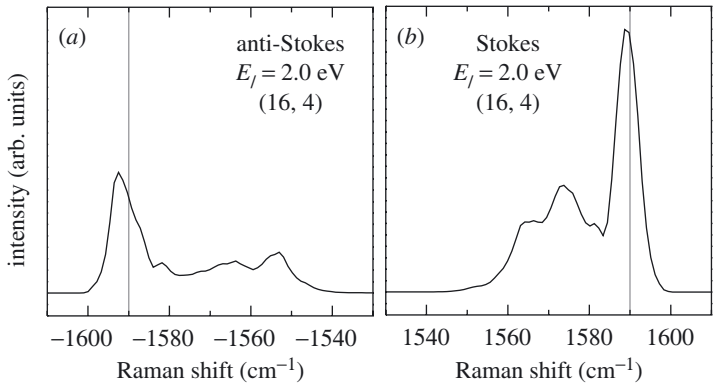

Figure 8. Calculated double-resonance (*a*) anti-Stokes and (*b*) Stokes Raman line shapes of a $(16, 4)$ nanotube excited at $\hbar\omega_{\mathrm{L}} = 2.0$ eV. It can easily be seen that both shape and intensity maxima are significantly different for the two processes compared with a single-resonance assumption, where they would scale by at most a simple factor. The vertical grey lines are drawn at ± 1590 cm^{-1} and emphasize the difference in the maxima of Stokes and anti-Stokes peaks. (Reproduced with permission from Reich *et al.* (2004).)

lens. Theoretically, we see from equation (3.1) that the matrix elements $\mathcal{M}$ of the numerator are needed for evaluation. The electron–phonon and electron–radiation matrix elements have been calculated by Machón *et al.* (2004*a*). This has not been done for the interaction of carriers with defects in carbon nanotubes, and the matrix element $\mathcal{M}_{\mathrm{e-def}}$ is unknown. Still, it is possible to compare the amplitude of the equivalent single-resonance process of equation (2.1) and state whether it has the right order of magnitude or is much too small. The latter would indicate that a higher-order process, such as a double resonance, is needed to explain the absolute magnitude of the Raman signal. A full analysis of this point is forthcoming.

(*d*) *Stokes and anti-Stokes spectra*

The difference in shape and frequency maxima in Stokes and anti-Stokes spectra was noticed in graphite by Tan *et al.* (1998) and is discussed by Reich & Thomsen (2004) (see also Reich *et al.* 2004; Zólyomi & Kürti 2002). We note here simply that the difference in Stokes and anti-Stokes spectra that (from a standard Raman point-of-view) should not exist is a consequence without further assumptions from the double-resonance process (Thomsen & Reich 2000). This can be seen easily from the schematic in figure 3. In the anti-Stokes process corresponding to figure 3*b*, a phonon is absorbed and the electron energy increased by the phonon energy (instead of being decreased, as in figure 3*b*). To scatter the electron into the band, the electron must obtain a larger k and hence a different phonon (one with larger wave vector) and, if dispersive, a different ω_{ph} is involved. As a consequence, the Raman spectrum looks different in Stokes and anti-Stokes. In figure 8, the calculated Stokes and anti-Stokes spectra of the high-energy mode of a $(16, 4)$ nanotube are shown. They display the characteristic differences in shape and maxima known from experiment (Brown *et al.* 2000). The differences in Stokes and anti-Stokes spectra constitute the sixth criterion for a double-resonance Raman process (for more details, see, for example, Reich *et al.* 2004).

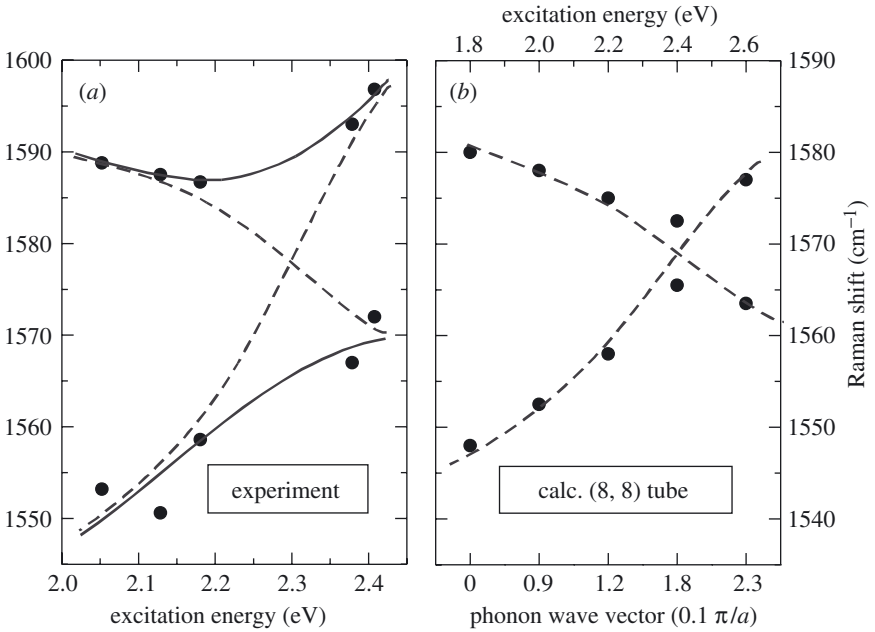

Figure 9. Excitation-energy dependence of the high-energy mode of an isolated carbon nanotube in double resonance. (*a*) Experimental values; the lines are guides to the eye. (*b*) Calculated excitation-energy dependence of the phonon frequencies of an $(8, 8)$ nanotube. The approximate phonon wave vector of the double-resonance phonon is given. Note that the wave vector scale is not linear. (After Maultzsch *et al.* (2003).)

(*e*) *Two optical-phonon dispersions in a carbon nanotube*

All of the characteristic ingredients (1)–(6) for a double resonance are thus more or less fulfilled in carbon nanotubes, and it should be possible to calculate reliably the excitation-energy dependent double-resonance Raman spectrum. Given the dispersion of the electronic bands of nanotubes involved in the absorption process (Reich *et al.* 2002) and the phonon dispersions (Maultzsch *et al.* 2002*b*), one can calculate the Raman spectrum from the sum in equation (3.1) and compare it with the experimentally found frequencies.

Such a comparison was performed by Maultzsch *et al.* (2003) and is shown in figure 9: the experiment on an isolated nanotube in part (*a*), the model calculation for an $(8, 8)$ metallic nanotube in (*b*). We will discuss the specifics of the metallic band structure of the $(8, 8)$ tube later, and state here the excellent agreement between theory and experiment. In particular, of the two high-energy modes, the upper one first decreases and then increases in energy for increasing photon excitation energy. The lower branch increases continuously in the range investigated. In an achiral (armchair or zig-zag) nanotube the corresponding branches have different symmetry, and hence they may cross as indicated by the dashed lines (guides to the eye). In a general chiral tube the two branches have the same symmetry and they must anti-cross (full lines), which appears to describe the data slightly better. Moreover, in achiral tubes phonons from one of these branches are forbidden by symmetry.

Note that this experiment was performed on an isolated nanotube such that the single-resonance view sometimes claimed to be dominant in the high-energy Raman

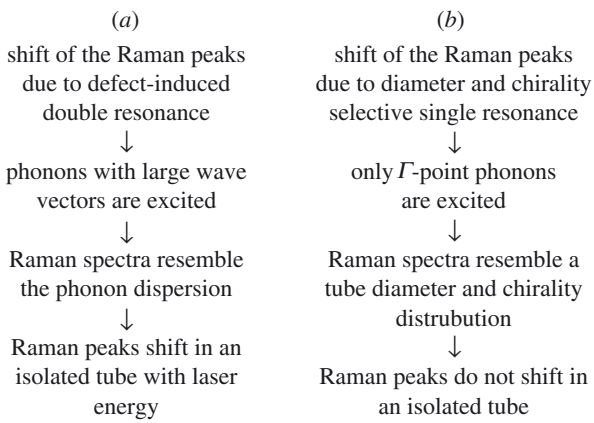

Figure 10. Flow chart summarizing the essential arguments distinguishing (*a*) the double-resonance process from (*b*) the single-resonance process. The excitation-dependent spectra on individual nanotubes presented by Maultzsch *et al.* (2003) (see figures 9 and 14) show that the double resonance is dominant in the high-energy spectra of carbon nanotubes. (After Thomsen (2003).)

process—namely that a different tube is selected out of an ensemble by a single resonance for each excitation energy—no longer holds. We summarize the arguments given for double resonance in an individual tube in the flow chart of figure 10 (Thomsen 2003). We feel that, together with the convincing experimental results, they prove beyond reasonable doubt that the high-energy mode is due to double resonance.

(*f*) *The electronic dispersion in relation to the double resonance*

Now we ask which is the underlying electronic band structure of carbon nanotubes where we observe double resonance. In figure 11 we show the electronic band structure of an armchair nanotube with the characteristic Fermi level crossing of the electronic bands at $\pm 2\pi/3a$ of the Brillouin zone. In graphite this point corresponds to the K-point. A and B mark two allowed optical transitions at the same photon energy between two different sets of bands. The transition between the two crossing bands is not allowed by symmetry. Transition A is thus the lowest transition in this particular band structure. Two possible double-resonance scattering processes are indicated in the figure, one with a large (compared with the Brillouin zone) wave vector (dashed arrow), and one with a smaller wave vector (say one-third of the Brillouin zone). The former process corresponds to the large-wave vector scattering involved in the D mode, while the latter shows up in the spectra as the high-energy mode. The second transition (B) has a similar but slightly larger D mode wave vector (not shown), but the high-energy wave vector is comparatively much smaller than for transition A, and the phonon involved is thus much closer to the Γ point than that involved in transition A. A small change in excitation energy can cause an upshift in one component of the high-energy mode while the other one experiences a downshift at the same time: depending on whether the phonon q is larger or smaller than the maximum in the overbending phonon dispersion, an increase in phonon wave vector is going to cause a frequency downshift or an upshift, respectively. We saw both of these features in figure 6.

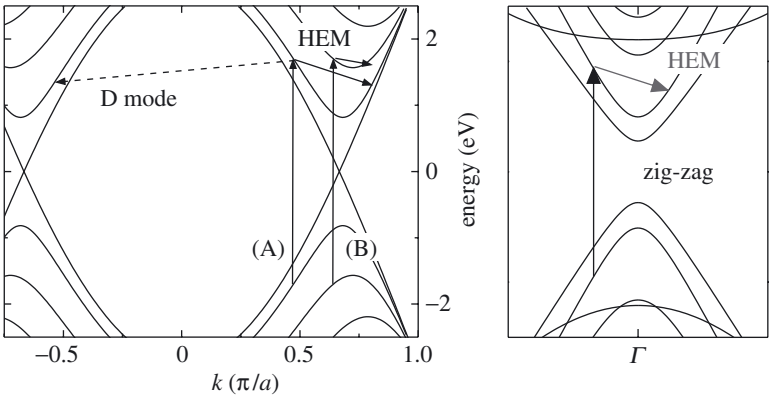

Figure 11. (*a*) Electronic band structure of an armchair carbon nanotube. The double-resonance process for the high-energy mode (HEM) is indicated by solid arrows following the absorbing transitions (A) or (B), the dashed line shows the resonant transition in case of the D mode. The defect-scattering process and the recombination are not shown. Transition B is into a higher band than transition A; correspondingly, the wave vector involved in the double resonance is smaller for B than for A and a different phonon energy expected for a dispersive phonon band. (*b*) Band structure of a zig-zag nanotube. The high-energy mode is doubly resonant here as well. The transition corresponding to the D mode cannot take place in the so-called $\mathcal{R} = 1$ nanotubes. See text for details. (After Maultzsch *et al.* (2001).)

In summary, we find the criteria for a double-resonance process of the high-energy mode fulfilled, most with rigour (criteria (1)–(4) and (6)), and one (5) qualitatively so far only. We have not mentioned a further important point, which is the symmetry of the high-energy mode. Experimentally it was shown to be mostly of A_1 symmetry (Duesberg *et al.* 2000; Reich *et al.* 2001*a*; Thomsen *et al.* 1999). The double-resonance process as described here involves only $A_{1(g)}$ phonons (see also figure 7) and is thus fully consistent with experiment. On the other hand, all phonon assignments based on single resonance are confined to the Γ point (by equation (2.2)) and necessarily include branches that are not of $A_{1(g)}$ symmetry (Rao *et al.* 1997). The significant presence of such modes can, however, be ruled out from experiment. There is thus convincing evidence that the high-energy mode is doubly resonant in carbon nanotubes.

5. ‘Metallic’ versus ‘semiconducting’ spectra

There is an interesting point in the shape of the Raman spectra in isolated tubes when they are excited with different excitation energies, as shown in figure 12. Going from $\hbar\omega_L = 2.05$ to 2.41 eV the line shape changes from what is generally considered to be a more ‘metallic’ line shape to one that is considered more ‘semiconducting’ (Pimenta *et al.* 1998; Rafailov *et al.* 2000). This notion was introduced because the ‘metallic’ line shape occurred for excitation energies where metallic nanotubes with typical diameter have their first singularity in the joint density of states. Several attempts that link the broader line shape and lower peak frequency to Fano resonances of the phonon with the metallic continuum have been published (see, for example, Brown *et al.* 2001; Jiang *et al.* 2002).

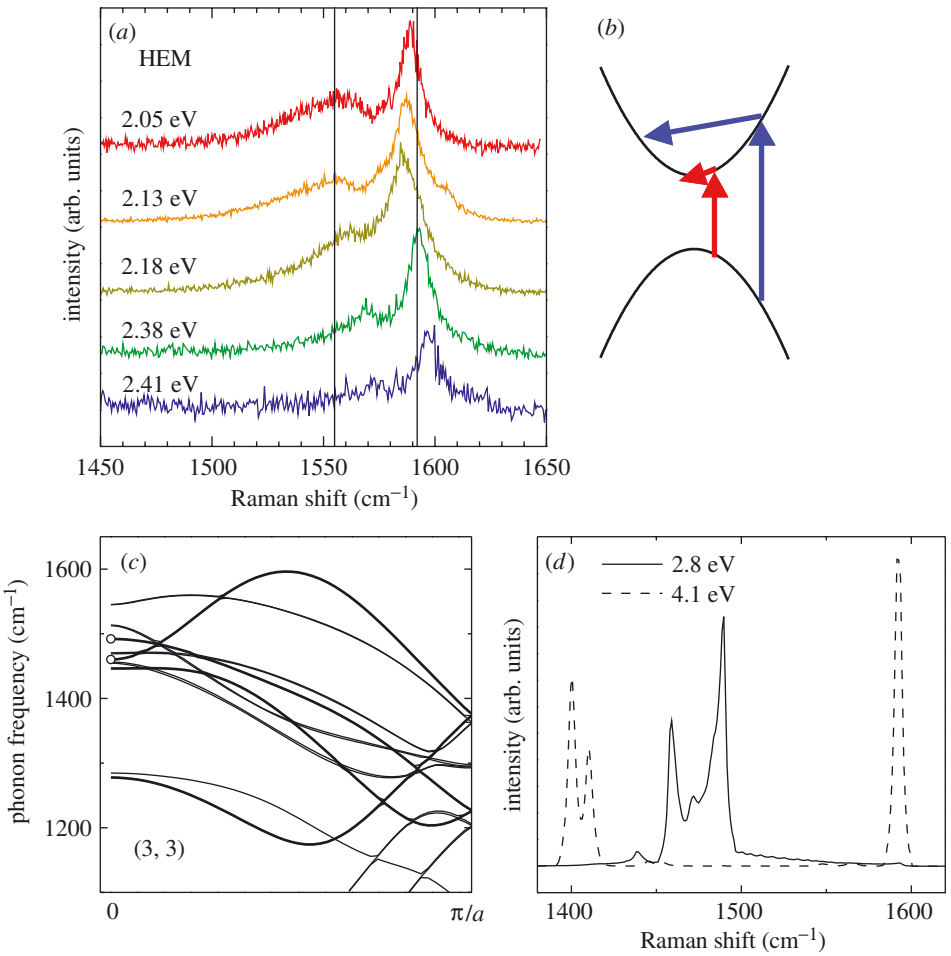

Figure 12. For increasing excitation energy the line shape of the isolated nanotube investigated in (*a*) appears to change continuously from 'metallic' looking to 'semiconducting' looking. (*b*) A schematic showing how this change in appearance may come about in a single (metallic) tube through double resonance and the larger phonon wave vectors involved with larger transition energies. (*c*) Calculated dispersion curves of a (3, 3) nanotube. (*d*) Calculated Raman spectrum of a (3, 3) nanotube for two different excitation energies, corresponding to the two transitions shown schematically in (*b*). The solid line resembles more the 'metallic' (Peierls softened) line shape of the high-energy mode, the dashed line that of a 'semiconducting' tube, although the (3, 3) nanotube is in fact metallic. (Reproduced with permission from Maultzsch *et al.* (2003), Thomsen (2003) and Maultzsch *et al.* (2002*d*).)

Apparently this argument falls into the simple single-resonance view (see also figure 10): different laser energies select different tubes from an ensemble of nanotubes; for some laser energies metallic nanotubes are present more in the Raman spectra than semiconducting ones; for other laser energies the reverse is true. We discuss this point explicitly because of its relevance to classifying nanotubes as metallic or semiconducting, which becomes important in all of the electronic applications of carbon nanotubes. The measurements on isolated nanotubes shown in figure 12 in the ensemble view should be a more or less linear superposition of a 'metallic' and a

'semiconducting' spectrum, with the 'semiconducting' one becoming stronger when going further from the metallic resonance. Instead, however, we find experimentally a nearly continuous transition from one line shape and one frequency to the other.

From a double-resonance point-of-view this may be well understood (see the schematic in figure 12*b*). For a particular metallic nanotube the band shown corresponds to the lowest one allowed to participate in an optical transition (see also figure 11). The phonon wave vectors involved in the double resonance are thus small and correspond to frequencies near the Γ point. These frequencies, in metallic nanotubes, have been calculated by Dubay *et al.* (2002) to soften significantly from the graphite value due to a Peierls-like mechanism. For a similar calculation, see figure 12*c*, from Maultzsch *et al.* (2002*d*). For excitation energies close to the minimum of the allowed band the small-q phonons with the softened energies contribute most to the double-resonance Raman spectra. This is seen in figure 12*d* (solid line), where we calculated the spectrum for a $(3, 3)$ nanotube with the Peierls-softened mode. For an excitation energy much larger than the band minimum in figure 12*b* we find the high-energy mode to have a more 'semiconducting' appearance (figure 12*d* dashed line): the phonon wave vector involved in the double resonance is large and the corresponding phonon frequency closer to the graphite frequency (Maultzsch *et al.* 2002*d*). Note that the actual tube measured in figure 12*a* is not a $(3, 3)$ tube; such small nanotubes grow only under special conditions (Wang *et al.* 2000). The calculation serves merely to demonstrate the effect of different excitation energies on metallic tubes. The softening of the Γ-point frequencies in metallic tubes and the Fano resonance have the same origin: the strong coupling of the phonon to the electronic system. A calculation of the Fano line shape requires non-Γ-point phonon wave vectors (Kempa 2002), consistent with the picture of double-resonance Raman scattering. As a consequence of the double resonance, a 'semiconducting' Raman spectrum can be due either to a semiconducting tube or to a metallic tube excited above the minimum of the bands involved in the optical transitions. A 'metallic' spectrum indicates a metallic tube.

6. The D mode

The D mode in carbon nanotubes as proposed by Maultzsch *et al.* (2001) is accepted as being a double-resonance process; this is probably because it has a similarly large excitation-energy dependent shift as the D mode in graphite (at *ca.* $50\ \mathrm{cm}^{-1}\ \mathrm{eV}^{-1}$). What is not always appreciated is that there is a selection rule that goes with the double resonance in carbon nanotubes. Namely, only nanotubes with an integer value of $(n_1 - n_2)/3n$ (so-called $\mathcal{R} = 3$ tubes) contribute to the D mode spectrum because of the particular electronic structure of those tubes. In other words, only those tubes fulfil appropriately criterion 1 and symmetry-imposed selection rules for the involvement of a D mode phonon. Other tubes (those with $\mathcal{R} = 1$) can also have a double-resonance process, but the phonons involved are close to the Γ point and thus are in the energy region of the high-energy mode. There is thus an ambiguity in the interpretation of first-order Raman spectra of isolated carbon nanotubes as regards the amplitude of the D mode peak: the absence (or small amplitude) of a peak in the D mode region could indicate a low defect concentration or the presence of an $\mathcal{R} = 1$ nanotube under the microscope. In order to get reliable information about the defect concentration, it is necessary to include the intensity of the second-order mode, which

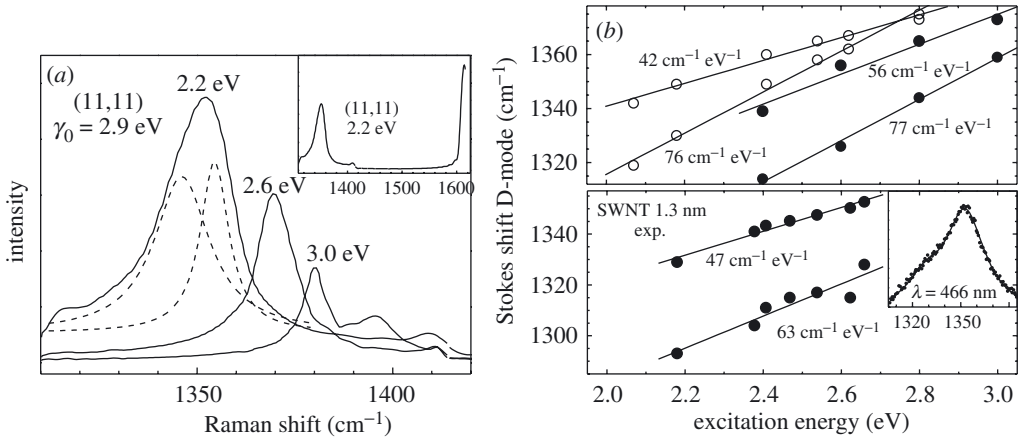

Figure 13. Calculated D mode Raman spectra for an (11, 11) nanotube for various excitation energies (*a*) (on an extended scale, inset) and a comparison of the experimental frequencies with the calculated ones; open symbols, (10, 10); closed symbols, (8, 8) (*b*, upper). Experimental frequency shifts with the average slopes of the two fitted components are given next to the curves (*b*, lower). Note the non-Lorentzian line shape in both the calculation and the experiment (*b*, inset). (Reproduced with permission from Maultzsch *et al.* (2001).)

is due to two-phonon processes and hence to first approximation independently of defect concentration (Maultzsch *et al.* 2002*c*).

We show in figure 13 the calculated D mode peaks for an (11, 11) nanotube for various excitation energies compared with a calculation based on double resonance from Maultzsch *et al.* (2001). It is nicely seen how the phonon shifts rapidly to higher energies, how its calculated line shape is not a single Lorentzian in both theory and experiment (see inset of figure 13*b* (lower)), and how its intensity decreases with increasing distance from the van Hove singularity. The experimental Raman intensity is of the order of that of the high-energy mode and thus also large (the D mode is detectable in individual nanotubes (Duesberg *et al.* 2000)). The expected differences in Stokes and anti-Stokes spectra were reported by Brown *et al.* (2000), and thus the experimental result fulfils all criteria put forward in order for double resonance to be the dominant process in D mode scattering. There have been several further investigations of the D mode based on double resonance; we refer to the literature for those studies (Kürti *et al.* 2002).

We mention here also the measurements of the D mode double resonance in isolated nanotubes. According to the flow chart in figure 10 the excitation-energy dependent shift should be present in isolated tubes just the same as in ensembles of tubes which is indeed the case. In figure 14 we show the D mode as derived from measurements of isolated nanotubes by Maultzsch *et al.* (2003). They show consistently the same numerical shift as known for the D mode of carbon nanotubes. For the D mode there is thus little doubt that its appearance in the Raman spectra is due to double-resonance scattering.

7. The RBM

We now turn briefly to the RBM. All interpretations of its frequency in the spectra have been based on the assumption that it is a Γ-mode frequency. In particular, the

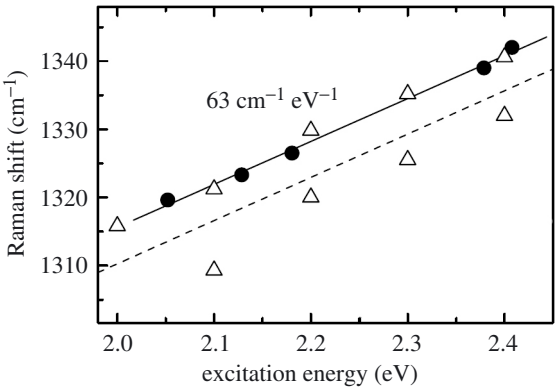

Figure 14. Experimental peak frequencies (solid symbols) in the D mode region of an isolated carbon nanotube and comparison with a calculation of the D mode in double resonance (open triangles). The experimental shift (63 cm^{-1}) is similar to that found in ensembles of tubes: a result which proves the applicability of double resonance to the analysis of the spectra. The two calculated sets of triangles correspond to two components in the calculated D mode. (After Maultzsch *et al.* (2003).)

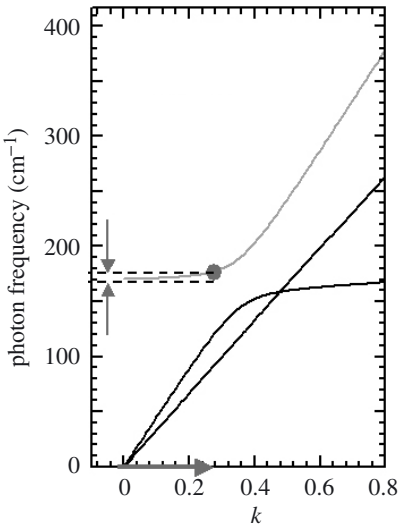

Figure 15. The double resonance may cause an apparent shift between the experimentally determined ω_{RBM} (solid circle) and the actual Γ-point frequency (intersection of the phonon dispersion with the ordinate at $k = 0$) needed in equation (7.1). (After Thomsen *et al.* (2003).)

well-known diameter–frequency relationship (Jishi *et al.* 1993; Kürti *et al.* 1998)

$$\omega_{\mathrm{RBM}} = \frac{C}{d} \tag{7.1}$$

is based on knowing the Γ-mode frequency, and not the frequency at a point somewhere in the Brillouin zone. We show the possible effect of double resonance on ω_{RBM} in figure 15; it is clear that for a typical double-resonance wave vector the frequency determined in a Raman experiment could deviate from the Γ-point frequency. Depending on the actual dispersion and the magnitude of the phonon wave

vector this could amount to somewhere between 1 and 10 cm^{-1}. The dispersion in figure 15 was calculated by Dobardžić *et al.* (2003); the frequency shift for a phonon wave vector of about one-third of the Brillouin zone leads to a shift of 10 cm^{-1}, as indicated by the opposing double arrows. In an attempt to use equation (7.1) for finding the diameter d of an investigated tube, this would yield a diameter too small by *ca.* 5% for a typical nanotube. In view of the *ca.* 5% uncertainty in the constant C (for a discussion of this point, see Reich *et al.* (2004)), this may not seem an excessive additional error; it should be kept in mind, though, that without correcting for the apparent shift due to double resonance one obtains systematically too small diameters from equation (7.1). Criterion 1 for the double resonance is thus fulfilled in case of the RBM.

What about the other characteristics of a double resonance? Criterion 3 has not yet been sufficiently systematically studied, to our knowledge, while criterion 2 could be fulfilled the same way as for the D mode and the high-energy mode. The line shape of the RBM (criterion 4) does not appear to deviate much from a Lorentzian. The line width is, however, much narrower than that of the high-energy mode, so that we cannot be sure of its Lorentzian nature. As for the absolute intensity of the RBM, the procedure outlined above to calculate the Raman intensity in single resonance and compare it with experiment was performed by Machón *et al.* (2004*b*). They found that the Raman intensity as calculated is one to two orders of magnitude smaller than those observed experimentally. In spite of the error associated with such a comparison, this can be taken as an indication that criterion 5 for a double resonance is fulfilled. And, finally, the Stokes–anti-Stokes difference in shape (criterion 6) is small because of the small phonon energy of the RBM.

To summarize, the RBM has not been proven to originate from a double-resonance process. There are indications, though, that it might, and further experiments on isolated nanotubes are needed to clarify this point, which will have notable consequences for the application of equation (7.1) to determine nanotube diameters.

8. Summary

We have presented an introduction to single and double resonances in the Raman spectroscopy of solids. We established six criteria which allow the identification of a double-resonance process over a single-resonance one. We then applied these criteria to the experimental results obtained for ensembles and isolated carbon nanotubes for the high-energy mode, the D mode and the RBM. We concluded that both the D mode and the high-energy mode are predominantly double-resonance processes, whereas there are only indications that the RBM is a double-resonance process. More work is needed to confirm this latter point.

S.R. was supported by the Berlin-Brandenburgische Akademie der Wissenschaften, the Oppenheimer Fund, and Newnham College. We thank the Deutsche Forschungsgemeinschaft for funding under Grant no. Th 662-8/2.

References

Brown, S. D. M., Corio, P., Marucci, A., Dresselhaus, M. S., Pimenta, M. A. & Kneipp, K. 2000 Anti-Stokes Raman spectra of single-walled carbon nanotubes. *Phys. Rev.* B **61**, R5137.

Brown, S. D. M., Jorio, A., Corio, P., Dresselhaus, M. S., Dresselhaus, G., Saito, R. & Kneipp, K. 2001 Origin of the Breit–Wigner–Fano lineshape of the tangential G-band feature of metallic carbon nanotubes. *Phys. Rev.* B **63**, 155414.

Cardona, M. 1982 Resonance phenomena. In *Light scattering in solids. II* (ed. M. Cardona & G. Güntherodt). Topics in Applied Physics, vol. 50, p. 19. Springer.

Dobardžić, E., Nikolić, I. M. B., Vuković, T. & Damnjanović, M. 2003 Single-wall carbon nanotubes phonon spectra: symmetry-based calculations. *Phys. Rev.* B **68**, 045408.

Dresselhaus, M. S., Dresselhaus, G. & Eklund, P. C. 1995 *Science of Fullerenes and carbon nanotubes*. Academic.

Dubay, O., Kresse, G. & Kuzmany, H. 2002 Phonon softening in metallic tubes by a Peierls-like mechanism. *Phys. Rev. Lett.* **88**, 235506.

Duesberg, G. S., Loa, I., Burghard, M., Syassen, K. & Roth, S. 2000 Polarized Raman spectroscopy of individual single-wall carbon nanotubes. *Phys. Rev. Lett.* **85**, 5436.

Fano, U. 1961 Effects of configuration interaction on intensities and phase shifts. *Phys. Rev.* **124**, 1866.

Friedl, B., Thomsen, C. & Cardona, M. 1990 Determination of the superconducting gap in $RBa_2Cu_3O_{7-\delta}$. *Phys. Rev. Lett.* **65**, 915.

Friedl, B., Thomsen, C., Habermeier, H.-U. & Cardona, M. 1991 Intensity anomaly of Raman active phonons in the superconducting state of $YBa_2Cu_3O_{7-\delta}$. *Solid State Commun.* **78**, 291.

Gaisler, V. A., Neizvestnyi, I. G., Singukov, M. P. & Talochkin, A. B. 1987 Raman scattering by surface vibrations of germanium crystals. *JETP Lett.* **45**, 441.

Gubarev, S. I., Ruf, T. & Cardona, M. 1991 Doubly resonant Raman scattering in the semimagnetic semiconductor $Cd_{0.95}Mn_{0.05}Te$. *Phys. Rev.* B **43**, 1551.

Jiang, C., Kempa, K., Zhao, J., Schlecht, U., Kolb, U., Basché, T., Burghard, M. & Mews, A. 2002 Strong enhancement of the Breit–Wigner–Fano Raman line in carbon nanotube bundles caused by plasmon band formation. *Phys. Rev.* B **66**, 161404(R).

Jiang, C., Zhao, J., Therese, H. A., Friedrich, M. & Mews, A. 2003 Raman imaging and spectroscopy of heterogeneous individual carbon nanotubes. *J. Phys. Chem.* B **107**, 8742.

Jishi, R. A., Venkataraman, L., Dresselhaus, M. S. & Dresselhaus, G. 1993 Phonon modes in carbon nanotubules. *Chem. Phys. Lett.* **209**, 77–82.

Jorio, A., Souza Filho, A. G., Dresselhaus, G., Dresselhaus, M. S., Saito, R., Hafner, J. H., Lieber, C. M., Matinaga, F. M., Dantas, M. S. S. & Pimenta, M. A. 2001 Joint density of electronic states for one isolated single-wall carbon nanotube studied by resonant Raman scattering. *Phys. Rev.* B **63**, 245416.

Jorio, A., Pimenta, M. A., Souza Filho, A. G., Samsonidze, G. G., Swan, A. K., Ünlü, M. S., Goldberg, B. B., Saito, R., Dresselhaus, G. F. & Dresselhaus, M. S. 2003 Resonance Raman spectra of carbon nanotubes by cross-polarized light. *Phys. Rev. Lett.* **90**, 107403.

Kastner, J., Pichler, T., Kuzmany, H., Curran, S., Blau, W., Weldon, D. N., Delamesiere, M., Draper, S. & Zanderbergen, H. 1994 Resonance Raman and infrared-spectroscopy of carbon nanotubes. *Chem. Phys. Lett.* **221**, 53.

Kempa, K. 2002 Gapless plasmons in carbon nanotubes and their interactions with phonons. *Phys. Rev.* B **66**, 195406.

Kürti, J., Kresse, G. & Kuzmany, H. 1998 First-principles calculations of the radial breathing mode of single-wall carbon nanotubes. *Phys. Rev.* B **58**, 8869.

Kürti, J., Zólyomi, V., Grüneis, A. & Kuzmany, H. 2002 Double resonant Raman phenomena enhanced by van Hove singularities in single-wall carbon nanotubes. *Phys. Rev.* B **65**, 165433.

Machón, M., Reich, S., Maultzsch, J., Ordejón, P. & Thomsen, C. 2004*a* Raman matrix elements of the high energy mode. In *Electronic properties of novel materials: progress in molecular nanostructures*. AIP Conference Proceedings, vol. 723, p. 381. Bethlehem, PA: American Institute of Physics.

Machón, M., Reich, S., Maultzsch, J., Ordejón, P. & Thomsen, C. 2004*b* The strength of the radial breathing mode in single-walled carbon nanotubes. Submitted.

Martin, R. M. & Falicov, L. M. 1983 Resonant Raman scattering. In *Light scattering in solids. I. Introductory concepts* (ed. M. Cardona), 2nd edn. Topics in Applied Physics, vol. 8, p. 79. Springer.

Maultzsch, J., Reich, S. & Thomsen, C. 2001 Chirality selective Raman scattering of the D mode in carbon nanotubes. *Phys. Rev.* B **64**, 121407(R).

Maultzsch, J., Reich, S. & Thomsen, C. 2002*a* Raman scattering in carbon nanotubes revisited. *Phys. Rev.* B **65**, 233402.

Maultzsch, J., Reich, S., Thomsen, C., Dobardžić, E., Milošević, I. & Damnjanović, M. 2002*b* Phonon dispersion of carbon nanotubes. *Solid State Commun.* **121**, 471.

Maultzsch, J., Reich, S., Thomsen, C., Webster, S., Czerw, R., Carroll, D. L., Vieira, S. M. C., Birkett, P. R. & Rego, C. A. 2002*c* Raman characterization of boron-doped multiwalled carbon nanotubes. *Appl. Phys. Lett.* **81**, 2647.

Maultzsch, J., Thomsen, C., Reich, S. & Machòn, M. 2002*d* Origin of the high-energy Raman modes in single-wall carbon nanotubes. In *Electronic properties of novel materials: progress in molecular nanostructures* (ed. H. Kuzmany, J. Fink, M. Mehring & S. Roth). AIP Conference Proceedings, vol. 633, p. 352. Bethlehem, PA: American Institute of Physics.

Maultzsch, J., Reich, S., Schlecht, U. & Thomsen, C. 2003 High-energy phonon branches of an individual metallic carbon nanotube. *Phys. Rev. Lett.* **91**, 087402.

Maultzsch, J., Reich, S., Thomsen, C., Requardt, H. & Ordejón, P. 2004 Phonon dispersion of graphite. *Phys. Rev. Lett.* **92**, 075501.

Mowbray, D., Fuchs, H., Niles, D., Cardona, M., Thomsen, C. & Friedl, B. 1990 Raman study of the Ge phonon side band. In *20th Int. Conf. on the Physics of Semiconductors* (ed. E. Anastassakis & J. Joannopoulos), p. 2017. World Scientific.

Pimenta, M. A., Marucci, A., Empedocles, S. A., Bawendi, M. G., Hanlon, E. B., Rao, A. M., Eklund, P. C., Smalley, R. E., Dresselhaus, G. & Dresselhaus, M. S. 1998 Raman modes of metallic carbon nanotubes. *Phys. Rev.* B **58**, R16016.

Rafailov, P. M., Jantoljak, H. & Thomsen, C. 2000 Electronic transitions in single-walled carbon nanotubes: a resonance Raman study. *Phys. Rev.* B **61**, 16179.

Rao, A. M. (and 12 others) 1997 Diameter-selective Raman scattering from vibrational modes in carbon nanotubes. *Science* **275**, 187.

Reich, S. & Thomsen, C. 2004 Raman spectroscopy of graphite. *Phil. Trans. R. Soc. Lond.* A **362**, 2271–2288.

Reich, S., Thomsen, C., Duesberg, G. S. & Roth, S. 2001*a* Intensities of the Raman active modes in single and multiwall nanotubes. *Phys. Rev.* B **63**, R041401.

Reich, S., Thomsen, C. & Ordejón, P. 2001*b* Eigenvectors of chiral nanotubes. *Phys. Rev.* B **64**, 195416.

Reich, S., Thomsen, C. & Ordejón, P. 2002 Band structure of isolated and bundled nanotubes. *Phys. Rev.* B **65**, 155411.

Reich, S., Thomsen, C. & Maultzsch, J. 2004 *Carbon nanotubes*. Wiley.

Ruf, T., Serrano, J., Cardona, M., Pavone, P., Pabst, M., Krisch, M., D'Astuto, M., Suski, T., Grzegory, I. & Leszczynski, M. 2001 Phonon dispersion curves in wurtzite-structure GaN determined by inelastic X-ray scattering. *Phys. Rev. Lett.* **86**, 906.

Saito, R., Jorio, A., Souza-Filho, A. G., Dresselhaus, G., Dresselhaus, M. S. & Pimenta, M. A. 2002 Probing phonon dispersion relations of graphite by double resonance Raman scattering. *Phys. Rev. Lett.* **88**, 027401.

Sapega, V., Cardona, M., Ploog, K., Irchenko, E. & Mirlin, D. 1992 Spin-flip Raman scattering in $GaAs/Al_xGa_{1-x}As$ multiple quantum wells. *Phys. Rev.* B **45**, 4320.

Schwoerer-Böhning, M., Macrander, A. T. & Arms, D. A. 1998 Phonon dispersion of diamond measured by inelastic X-ray scattering. *Phys. Rev. Lett.* **80**, 5572.

Skákalová, V., Hulman, M., Fedorko, P., Lukác, P. & Roth, S. 2003 Effect of γ-irradiation on SWNT. In *Electronic properties of novel materials: progress in molecular nanostructures* (ed. H. Kuzmany, J. Fink, M. Mehring & S. Roth). AIP Conference Proceedings, vol. 685, p. 143. College Park, MD: American Institute of Phyiscs.

Tan, P.-H., Deng, Y.-M. & Zhao, Q. 1998 Temperature-dependent Raman spectra and anomalous Raman phenomenon of highly oriented pyrolytic graphite. *Phys. Rev.* B **58**, 5435.

Thomsen, C. 2000 Second-order Raman spectra of single and multi-walled carbon nanotubes. *Phys. Rev.* B **61**, 4542.

Thomsen, C. 2003 *Raman scattering in carbon nanotubes.* Proceedings SPIE, vol. 5219, p. 45. Chicago, IL: International Society of Optical Engineers.

Thomsen, C. & Reich, S. 2000 Double-resonant Raman scattering in graphite. *Phys. Rev. Lett.* **85**, 5214.

Thomsen, C., Reich, S., Rafailov, P. M. & Jantoljak, H. 1999 Symmetry of the high-energy modes in carbon nanotubes. *Physica Status Solidi* B **214**, R15.

Thomsen, C., Maultzsch, J. & Reich, S. 2003 Double-resonant Raman scattering in an individual carbon nanotube. In *Electronic properties of novel materials: progress in molecular nanostructures* (ed. H. Kuzmany, J. Fink, M. Mehring & S. Roth). AIP Conference Proceedings, vol. 685, p. 225. Bethlehem, PA: American Institute of Physics.

Tuinstra, F. & Koenig, J. L. 1970 Raman spectrum of graphite. *J. Chem. Phys.* **53**, 1126.

Vidano, R. P., Fischbach, D. B., Willis, L. J. & Loehr, T. M. 1981 Observation of Raman band shifting with excitation wavelength for carbons and graphites. *Solid State Commun.* **39**, 341.

Wang, Y., Alsmeyer, D. C. & McCreery, R. L. 1990 Raman spectroscopy of carbon materials: structural basis of observed spectra. *Chem. Mater.* **2**, 557.

Wang, N., Tang, Z. K., Li, G. D. & Chen, J. S. 2000 Single-walled 4 Å carbon nanotube arrays. *Nature* **408**, 50.

Zólyomi, V. & Kürti, J. 2002 Calculating the discrepancy between the Stokes and anti-Stokes Raman D band of carbon nanotubes using double resonance theory. *Phys. Rev.* B **66**, 073418.